Evaluation of Fast-Time Wake Vortex Models using Wake Encounter Flight Test Data

Nash'at N. Ahmad[*], Randal L. VanValkenburg[†], Roland L. Bowles[‡]
NASA Langley Research Center, Hampton, Virginia, 23681

Fanny M. Limon Duparcmeur[§]
Craig Technologies Inc., Hampton, Virginia, 23681

Thijs Gloudesman[**], Sander van Lochem[††], Eelco Ras[‡‡]
Delft University of Technology, Delft, the Netherlands

This paper describes a methodology for the integration and evaluation of fast-time wake models with flight data. The National Aeronautics and Space Administration conducted detailed flight tests in 1995 and 1997 under the Aircraft Vortex Spacing System Program to characterize wake vortex decay and wake encounter dynamics. In this study, data collected during Flight 705 were used to evaluate NASA's fast-time wake transport and decay models. Deterministic and Monte-Carlo simulations were conducted to define wake hazard bounds behind the wake generator. The methodology described in this paper can be used for further validation of fast-time wake models using en-route flight data, and for determining wake turbulence constraints in the design of air traffic management concepts.

Nomenclature

APA	=	AVOSS Prediction Algorithm
AVOSS	=	Aircraft Vortex Spacing System
ATM	=	Air Traffic Management
EDR	=	Eddy Dissipation Rate (ft^2/s^3)
TKE	=	Turbulence Kinetic Energy (ft^2/s^2)
TDP	=	TASS Driven Algorithms for Wake Prediction
TASS	=	Terminal Area Simulation System
Γ	=	vortex circulation (ft^2/s)
Γ_0	=	initial vortex circulation (ft^2/s)
V_0	=	initial vortex descent velocity (ft/s)
b_0	=	initial vortex pair separation (ft)
y_0	=	initial vortex pair lateral offset from a reference point (ft)
z_0	=	initial vortex pair vertical offset from a reference point (ft)
N	=	dimensional Brunt-Väisälä frequency (s^{-1})
N^*	=	non-dimensional Brunt-Väisälä frequency = $Nb_0V_0^{-1}$
ε	=	dimensional eddy dissipation rate (ft^2/s^3)
ε^*	=	non-dimensional eddy dissipation rate = $(\varepsilon b_0)^{1/3}V_0^{-1}$
θ	=	potential temperature/theta (K)

[*] Research Aerospace Engineer, NASA, Hampton, Virginia. Senior Member, AIAA.
[†] Research Scientist, NASA, Hampton, Virginia. Member, AIAA.
[‡] NASA Distinguished Research Associate, NASA, Hampton, Virginia. Member, AIAA.
[§] Research Scientist, Craig Technologies, Inc., Hampton, Virginia. Member, AIAA.
[**] Student Intern, Delft University of Technology, Delft, the Netherlands.
[††] Student Intern, Delft University of Technology, Delft, the Netherlands.
[‡‡] Student Intern, Delft University of Technology, Delft, the Netherlands.

T = temperature (°F)
T_L = Sarpkaya time-to-link
u = east-west velocity component (ft/s)
v = north-south velocity component (ft/s)
ρ = air density (sl/ft^3)
Δt_e = vortex encounter time (s)
Δx = distance between generator and follower at time of encounter (nmi)
g = acceleration due to gravity (ft/s^2)
W_G = weight of the generator (lb)
b_F = follower wing span (ft)
b_G = generator wing span (ft)
$\bar{Y}_F$ = y-coordinate of follower's center of gravity normalized by b_G
$\bar{Z}_F$ = z-coordinate of follower's center of gravity normalized by b_G
$\bar{s}$ = half of vortex pair separation (b_0) normalized by b_G
$\bar{r}_c$ = vortex core radius size normalized by b_G
I_{xx} = roll moment of inertia (sl·ft^2)
λ_F = wing taper ratio of the follower
V_F = follower airspeed (ft/s)
V_G = generator airspeed (ft/s)
q = free-stream dynamic pressure (lb/ft^2)
C_{l_v} = vortex-induced rolling moment coefficient
$C_{L_\alpha F}$ = three-dimensional lift curve slope of the follower
C_{l_c} = pilot input roll control corresponding to maximum aileron deflection
$C_{l_{\bar{p}}}$ = roll damping coefficient
ϕ = bank angle (deg)
ϕ_∞ = maximum bank angle of the aircraft without control input (deg)
ϕ_{max} = maximum vortex-induced bank angle (deg)

I. Introduction

The National Aeronautics and Space Administration (NASA) is developing fast-time wake transport and decay models to safely enhance the capacity of the National Airspace System (NAS). These models are empirical algorithms used for real-time predictions of wake transport and decay based on aircraft parameters and ambient weather conditions. The fast-time wake models can be used for the systems level design of advanced air traffic management (ATM) concepts that safely increase the capacity of the NAS. It is also envisioned that at some later stage of maturity, these models could be used operationally, not only within the terminal airspace but also as onboard tools to support concepts such as dynamic separation of aircraft.

The initial conditions of fast-time models (weather and aircraft parameters) can have large uncertainties (Pruis and Delisi 2011), which make it difficult to use deterministic predictions of point vortices in ATM applications. A probabilistic model takes into account these uncertainties in initial conditions and is also more suited for ATM applications. In ATM concepts development, the definition of wake hazard bounds in terms of wake strength and location is required. Previous research on probabilistic modeling of wakes and its integration with ATM applications include Holzäpfel (2003) and Gerz et al. (2007). Pruis and Delisi (2011) have developed a multi-model ensemble which gives bounded solutions for both wake strength and location. In this study both deterministic and Monte-Carlo solutions were used to evaluate the fast-time models. In addition, an aircraft-based wake encounter metric was integrated with fast-time models.

Several studies have been conducted in the past using lidar data to evaluate fast-time models in the terminal area setting (Proctor 2009; Pruis and Delisi 2011; Feigh et al. 2012; Ahmad et al. 2014). Although the risk of an inadvertent wake encounter is higher in the terminal area, such encounters can also occur at higher altitudes in the en-route environment. In this study, wake encounter data collected during flight tests are used to evaluate the fast-time wake models. In the following sections, the fast-time models and their integration for air traffic management

applications is described. The flight tests are described briefly and the evaluation of fast-time models (deterministic and Monte-Carlo simulations) with flight test data is discussed in detail.

II. Fast-Time Wake Vortex Modeling

The first fast-time wake transport and decay model was developed by Greene (1986). Some of the fast-time models currently in use include: AVOSS (Aircraft Vortex Spacing System) Prediction Algorithm (APA), TASS (Terminal Area Simulation System) Derived Algorithms for Wake Prediction (TDP), Probabilistic 2-Phased (P2P) model and the Deterministic wake Vortex Model (DVM). The APA and TDP models have been developed by NASA, while the P2P model (Holzäpfel 2003) and the DVM (de Visscher et al. 2010) have been developed by the Deutsches Zentrum für Luft- und Raumfahrt (DLR) and Université catholique de Louvain (UCL), respectively.

In the late 1990s, under NASA's AVOSS project (Perry et al. 1997; Hinton 2001), significant improvements were made in the fast-time wake modeling based on the data from field experiments and large eddy simulations. The APA model computes the out-of-ground-effect (OGE) decay and descent based on Sarpkaya (2000) and Sarpkaya et al. (2001). The lateral vortex transport is computed based on the vertical profile of crosswind (Robins and Delisi 2002). The model has an algorithm for enhanced rate of decay during the ground effect developed by Proctor et al. (2000). The in-ground-effect (IGE) transport accounts for vortex spreading and rebound (Robins et al. 2002). The TDP model (Proctor et al. 2006) replaces the Sarpkaya OGE decay module with algorithms developed from parametric studies using the TASS model (Proctor 1987) and includes the effect of the crosswind shear gradient on transport.

The initial conditions for the fast-time wake models are based on aircraft parameters and the ambient weather conditions. The aircraft dependent parameters include the initial values of vortex descent velocity (V_0) and vortex pair separation distance (b_0), and position of the aircraft. The atmospheric initial conditions include vertical profiles of either temperature or potential temperature (θ), eddy dissipation rate (ε), and crosswind. The model output consists of time histories of wake circulation strength and location (Figure 1). Various evaluations of the fast-time models have concluded that in general the errors in model circulation predictions have an average root mean square error on the order of $0.2\Gamma_0$ to $0.3\Gamma_0$ (Γ_0 is the initial wake circulation). The vertical transport errors are on the order of $0.5b_0$ and the lateral transport errors are on the order of b_0. The lateral transport errors can be reduced to as low as $0.5b_0$ if more accurate crosswind initial conditions (e.g., by using proxy crosswinds as initial conditions) are provided to the fast-time models (Pruis et al. 2011).

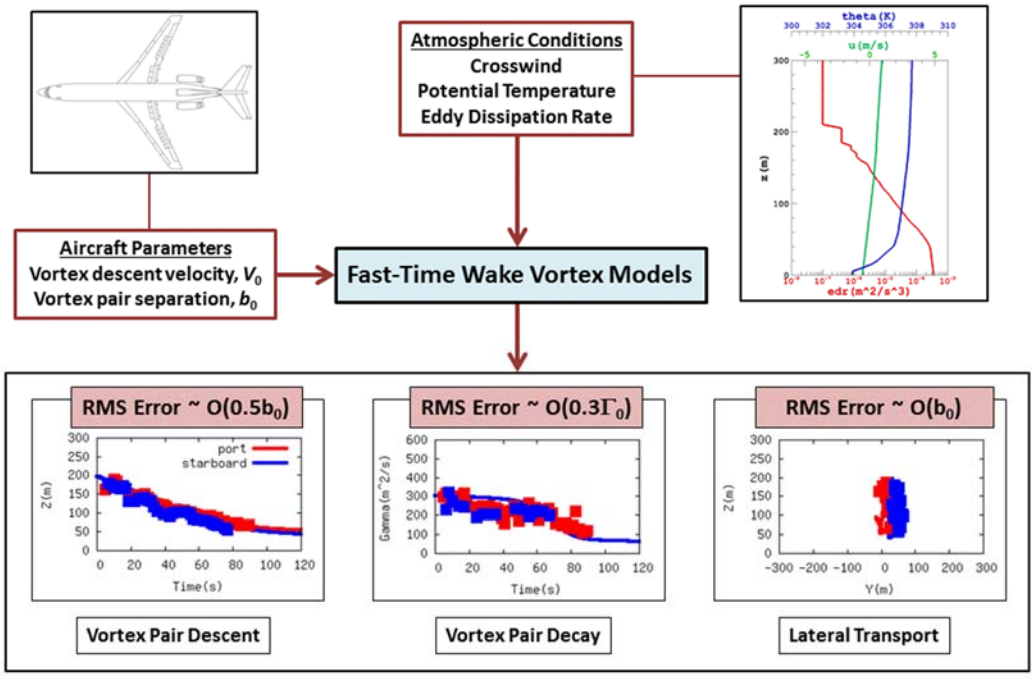

Figure 1. The flowchart shows the fast-time wake model inputs and outputs (MKS units). The average root mean square (RMS) errors in the model prediction of vortex circulation strength and location are also given.

III. NASA's Wake Vortex Flight Tests

A series of wake vortex flight tests (Reimer and Vicroy 1996; Vicroy et al. 1998; Vicroy et al. 1999) were conducted by NASA in the vicinity of Wallops Island, Virginia during 1995 and 1997 under the AVOSS Program. The generator aircraft used in the tests was a Lockheed-Martin C-130 (Figure 2). All flights were flown with flaps up and the gear retracted (clean configuration). Smoke canisters were installed on the wingtips for wake visualization. NASA Langley's OV-10A (Figure 2) was instrumented to take meteorological measurements and to probe the wakes generated by the C-130 (Stuever et al. 1995). A set of three booms (one on each wingtip and one on the right side of the nose) were mounted for taking measurements of position, velocities, pressure, temperature, and dew point temperature. Some characteristics of the aircraft are listed in Table 1. The general flight test sequence for the OV-10A was as follows (Vicroy et al. 1998):

- Turbulence Runs: Level flight with a constant heading at 1000ft below the test altitude.
- Weather Runs: Constant speed, constant heading climb from 1000ft below to 500ft above the test altitude.
- Turbulence Runs: Level flight with a constant heading at 500ft above the test altitude.
- Wake Vortex Runs: Series of penetrations into the C-130 wakes at various distances from the generator.
- A set of Turbulence and Weather Runs was repeated after the wake measurements.

The flight tests were conducted between 2000ft and 8000ft. Each OV-10A flight test database consists of several sub-datasets. The main run data is at a rate of 32Hz and includes the entire OV-10A flight. The wake encounter data was measured at 128Hz during the encounter runs. A digital camera was mounted on the tail of the OV-10A to capture images of wake encounters. The final database for each flight test contains more than 180 parameters (weather, wake, and aircraft response).

Table 1: Aircraft Parameters

Aircraft	Wing Span	Aspect Ratio	Taper Ratio	MTOW
C-130	132.6ft	10.08	0.857	155,000lb
OV-10A	40.0ft	5.50	1.000	14,400lb

The database includes several wake parameters which were computed from the measurements. These parameters include: the C-130 altitude and position (latitude/longitude) at the time of wake creation, range between OV-10A and C-130, as well as the true airspeed, heading, and weight of the C-130. The initial wake descent velocity is also included in the database. The OV-10A related parameters include detailed aircraft response (location, altitude, attitude, true air speed, etc.) during the wake encounters.

Data were collected at a rate of 128Hz in the weather runs. Examples of the potential temperature and wind speed/direction measured by the OV-10A in two of the weather runs for Flight 705 are shown in Figures 3 and 4. Special upper air soundings were taken in each of the flight test. These soundings were in addition to the National Weather Service 0000UTC and 1200UTC soundings taken at the Wallops Flight Facility. Analysis of meteorological conditions for some of the flight tests is given in Zak and Rodgers (1997).

Figure 2. Lockheed Martin C-130 (left), and the instrumented Rockwell North American OV-10A (right).

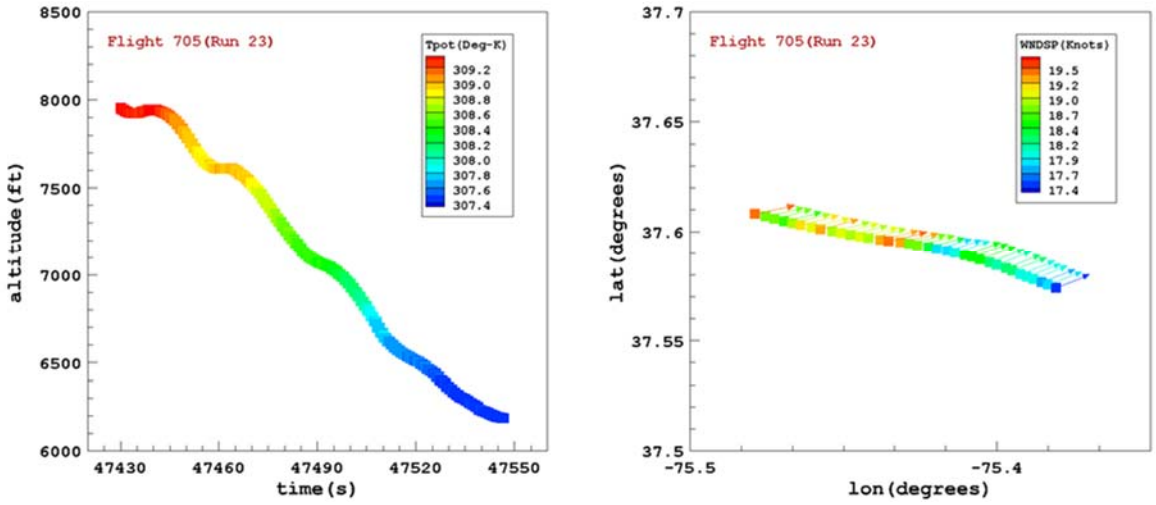

Figure 3. Flight Test 705. Weather Run 23. The left panel shows the OV-10A's descent in time and the right panel shows the flight path in the latitude-longitude space. The arrows give the ambient wind direction and are colored by wind speed. Wind data in the right panel are plotted every 100 points. August 13, 1997.

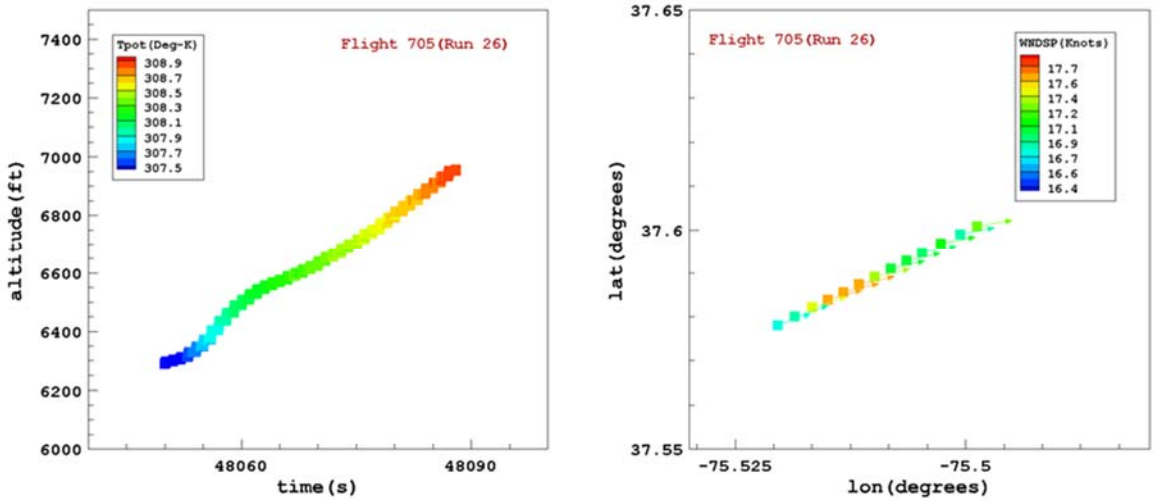

Figure 4. Flight Test 705. Weather Run 26. The left panel shows the OV-10A's ascent in time and the right panel shows the flight path in the latitude-longitude space. The arrows give the ambient wind direction and are colored by wind speed. Wind data in the right panel are plotted every 100 points. August 13, 1997.

IV. Results

In this section, the evaluation of the fast-time models using data from two different runs of Flight 705 is described in detail. The flight trajectories of Runs 28 and 37 are shown in Figure 5. The weather summary for Flight 705 is given in Table 2. Weather conditions for this day were hazy, with low turbulence levels (negligible on the MacCready scale – see Appendix A) and stable stratification. The non-dimensional eddy dissipation rate (ε^*) was on the order of 0.04, which resulted in the Sarpkaya time-to-link (T_L) of 5.26. The non-dimensional Brunt-Väisälä frequency (N^*) was in the range of 0.3-0.4 (weakly stable environment that can result in long-lasting wakes).

Pilot's notes indicate that the onset of Crow instability occurred after 5nmi (Vicroy et al. 1998). The first undulations in the wake during Run 28 were observed 3nmi in-trail. There were vertical undulations of ±20ft at 4.2nmi (lateral undulations were not present at this time). At 4.8nmi wake undulations in both vertical and lateral directions were observed. The first vortex bursting was observed at 6nmi. During Run 37 small undulations were

observed up to 6.2nmi behind the C-130 with vortex burst occurring after 6.5nmi. Rising vortices were also observed 1.5nmi behind the C-130 during Run 37. Zak and Rodgers (1997) have documented the meteorology associated with some of the observations of rising vortices during the flight tests.

Table 2: Flight Test 705 Weather Summary (Vicroy et al. 1998)

Parameter	Flight 705
Date	1997-08-13
Altitude(ft)	6200 – 8000
N(s^{-1})	0.01 – 0.015
TKE(ft^2s^{-2})	0.4 – 3.4
ε(ft^2s^{-3})	0.00002
MacCready Category	Negligible

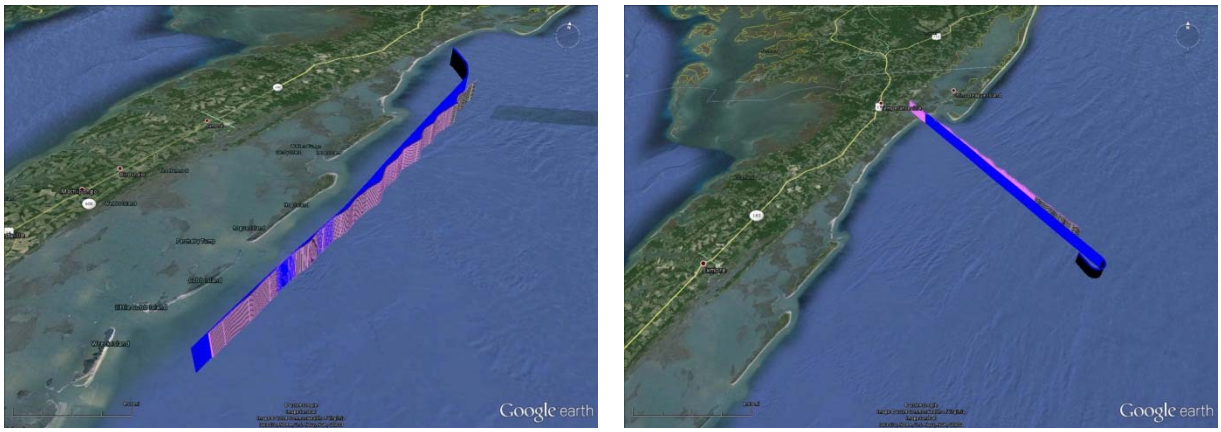

Figure 5. Flight 705. Run 28 (left), and Run 37 (right). C-130 (blue) and OV-10A (magenta) trajectories are shown in the figure.

A. Deterministic Runs

The current software design of the fast-time models assumes operations in the terminal area. For example, the initial lateral position of the vortex pair (y_0) is treated as an offset with respect to the runway centerline. For this study, software was developed to process flight data in latitude-longitude space with appropriate coordinate transformations, in order to make it more general purpose. The input stream included aircraft parameters of location (latitude, longitude, altitude), and the initial vortex descent rate (V_0) along the flight path. The initial vortex descent rate can be estimated from the aircraft weight, aircraft speed, air density, and the initial vortex separation b_0,

$$V_0 = \frac{W_G}{2\pi\rho V_G b_0^2} \tag{1}$$

where ρ is the air density, V_G is the generator true airspeed, and W_G is the generator weight. The initial separation distance between the vortices b_0 is based on the assumption of an elliptical wing loading,

$$b_0 = \frac{\pi}{4} b_G \tag{2}$$

where b_G is the wingspan of the generator. The wind speed, wind direction, and the generator heading were provided in the flight data and the crosswinds were estimated from these parameters along the entire flight path. The Brunt-Väisälä frequency and the ambient turbulence (eddy dissipation rate) were estimated from the OV-10A weather and turbulence runs (Table 2).

Two sets of simulations were performed. In the first set, an instance of fast-time models was initialized every second along the C-130 trajectory, using the y_0, z_0, V_0 and crosswinds at that location (Figure 6). In the second set of simulations, averaged values of V_0 and crosswinds along the entire trajectory were used (Figure 7). In Figure 7 the predictions of circulation decay by APA3.4 and TDP2.1 for Run 28 and Run 37 are compared with observations. The non-dimensional decay curves used for comparisons were estimated from OV-10A data taken during wake encounters (Vicroy et al. 1998). The estimated decay rate from observations for Run 28 was -0.025 and -0.015 for Run 37. These are very low decay rates which are sustained until a non-dimensional time of around 4 according to the estimates from observations.

TDP2.1 was able to predict the wake decay for Run 28 almost exactly for non-dimensional times up to approximately 2, but its decay rate becomes higher than observations after that. In Run 37 the TDP2.1 again performs well initially but differences appear after non-dimensional time of around 1. The APA3.4 predicts a much higher decay rate compared to observations. Previous evaluations of fast-time models using lidar data have also demonstrated more accurate TDP2.1 predictions compared to those of APA3.4 under stratified conditions.

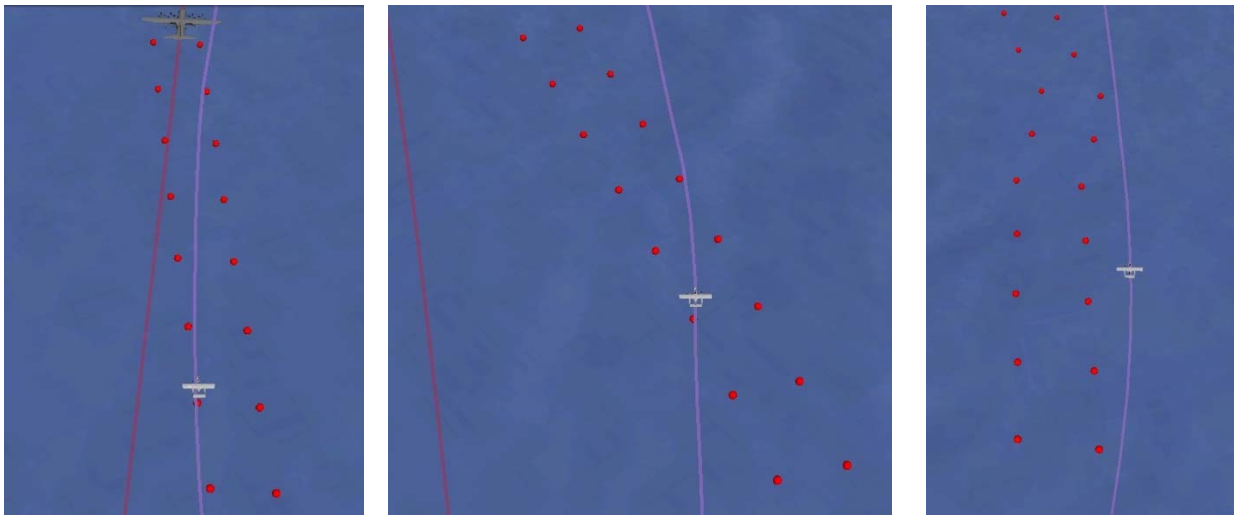

Figure 6. Run 28. An instance of TDP2.1 was initialized every second in the simulation shown in the figure.

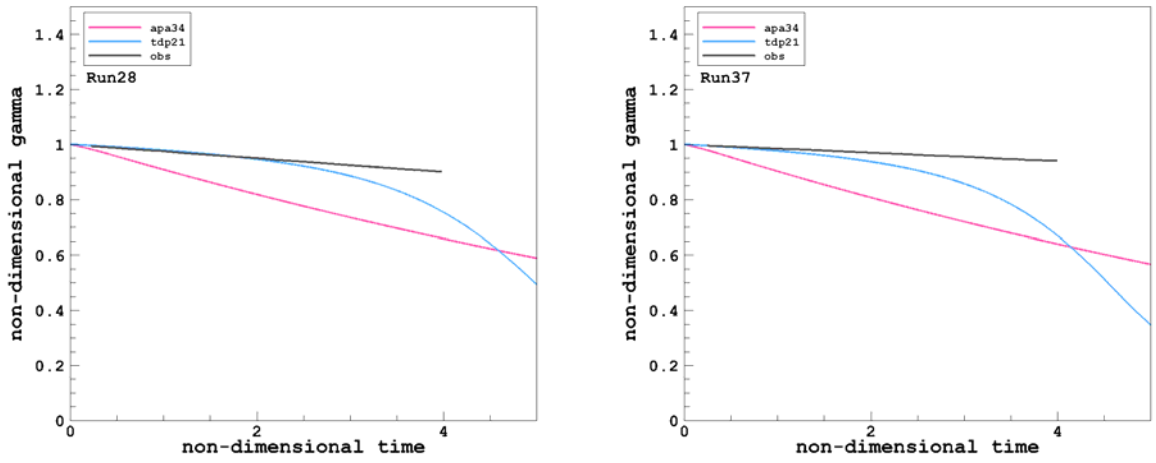

Figure 7. The non-dimensional circulation decay predicted by TDP21 and APA34 models for Run 28 (left) and Run 37 (right). The black line represents the linear fit to the observed data.

B. Monte-Carlo Simulations

The initial conditions of fast-time models can have large uncertainties. These uncertainties are not limited to the ambient weather conditions. Pruis and Delisi (2011) have pointed out that aircraft-related initial conditions can also introduce substantial uncertainties in the solutions calculated by the fast-time wake models. A statistical approach not only takes into account these uncertainties but is also more practical for ATM applications. In ATM concepts development, the definition of a bounded region where a hazardous wake may exist is more useful than the trajectories of point vortices obtained from deterministic simulations. In addition to deterministic runs, Monte-Carlo simulations were conducted to evaluate the models for Runs 28 and 37. The general methodology used is described in Appendix B. Previous applications of Monte-Carlo method with APA and TDP fast-time wake models include Pruis and Delisi (2011) and Johnson et al. (2013).

Normal distributions (2σ = 8.2-12.5ft/s) were used for crosswind (Holzäpfel 2013) with the mean set to the average crosswind for the entire run. The eddy dissipation rate was bounded within one order of magnitude around the mean (set to the measured value of $0.00002 ft^2/s^3$). The measured values of the Brunt-Väisälä frequency ranged between $0.01\text{-}0.015 s^{-1}$ for Flight 705. The Weather Research and Forecast (WRF) model was run to obtain the Brunt-Väisälä frequency for Flight 705. The WRF predictions of stratification agreed well with the observations (Appendix C), therefore for the Monte-Carlo simulations, a uniform distribution was used for the Brunt-Väisälä frequency, bounded between the observed values.

In addition to uncertainties in weather, the uncertainties in aircraft parameters were also taken into account. Perturbations for y_0 were generated using a normal distribution with σ=82ft (25m). Similarly for z_0, a normal distribution was used with mean set to z_0 and σ=33ft (10m), where z_0 is the average altitude for the entire run. The σ values for position were taken from Holzäpfel (2013). The flight test data includes the estimates of the weight and the true air speed of the generator as well as estimates of the initial vortex descent velocity (V_0) along the flight path. Probability density functions for V_0 were defined from this data (Figure 8) and used to generate perturbations in V_0. Delisi et al. (2013) have shown that although the value of b_0 for most commercial aircraft is close to estimates based on elliptical wing loading, there are some which are non-elliptical. For this research and due to limited data, b_0 was set to a constant value based on the elliptical wing loading.

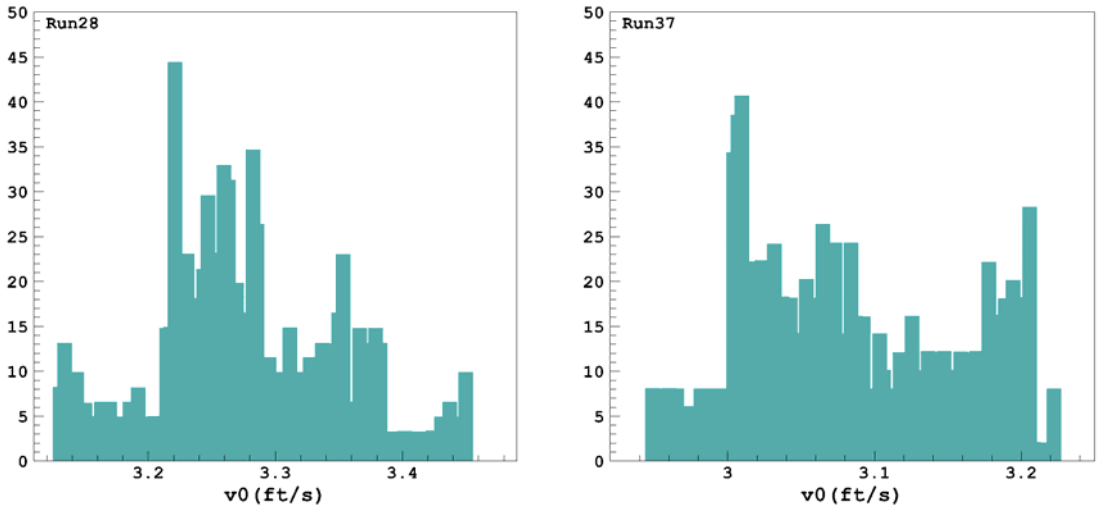

Figure 8. Variation in initial vortex pair velocity, V_0 for Run 28 (left panel) Run 37 (right panel).

Figures 9 through 11 show the results of Monte-Carlo simulations for Run 28. In general, the vortex location was well bounded within 2σ for both APA3.4 and TDP2.1. The circulation decay followed a similar pattern of deterministic runs with TDP2.1 predicting the decay rate with good accuracy for non-dimensional time of around 3. Figures 12-14 show the results of Monte-Carlo simulations for Run 37. The vortex location was well bounded by both TDP2.1 and APA3.4 predictions for this case as well. A normal distribution with 2σ = 8.2ft/s was used for crosswind in these simulations. Sensitivity runs with normal distribution using 2σ = 12.5ft/s for crosswinds gave better bounds for lateral position at later times (Figure 15).

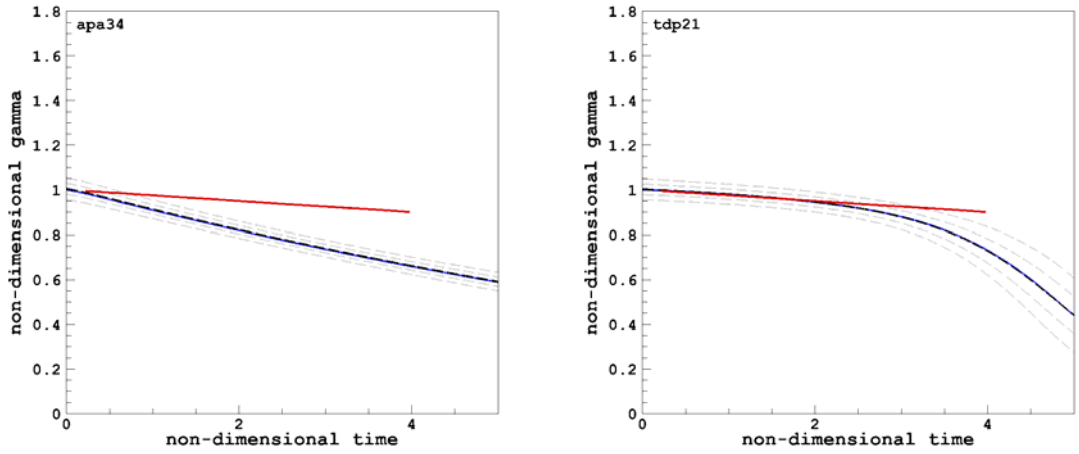

Figure 9. Run 28. Circulation decay predicted by APA34 and TDP21 models. Observations are given by the red line, deterministic solution in blue, mean by the black dashed line and [σ:2σ] bounds by the dashed gray lines.

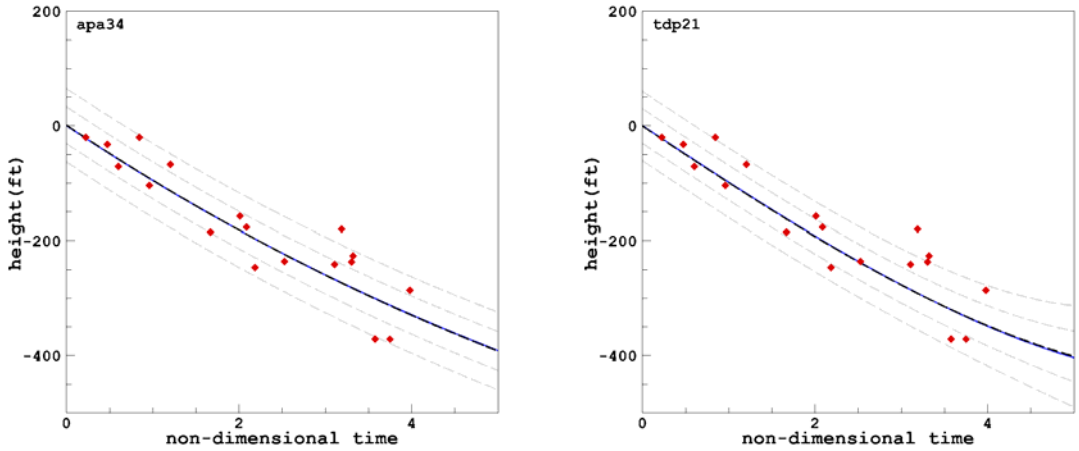

Figure 10. Run 28. Vortex descent predicted by APA34 and TDP21 models. Observations are given by the points, deterministic solution in blue, mean by the black dashed line and [σ:2σ] bounds by the dashed gray lines.

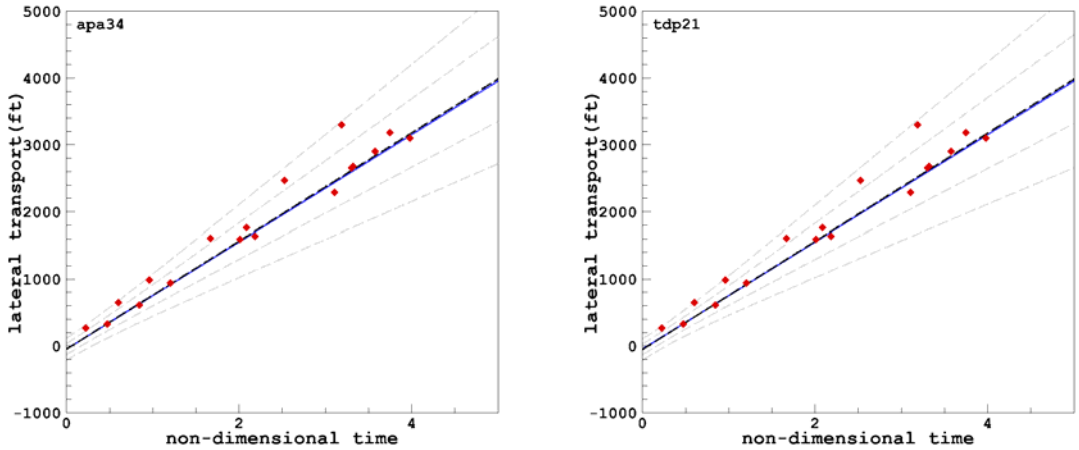

Figure 11. Run 28. Vortex transport predicted by APA34 and TDP21 models. Observations are given by the points, deterministic solution in blue, mean by black dashed line and [σ:2σ] bounds by the dashed gray lines.

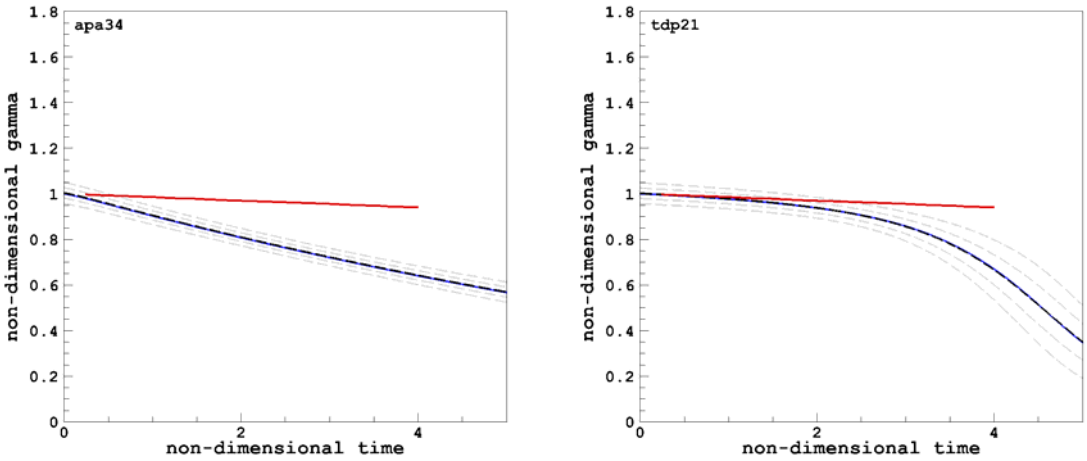

Figure 12. Run 37. Circulation decay predicted by APA34 and TDP21 models. Observations are given by the red line, deterministic solution in blue, mean by black dashed line and [σ:2σ] bounds by the dashed gray lines.

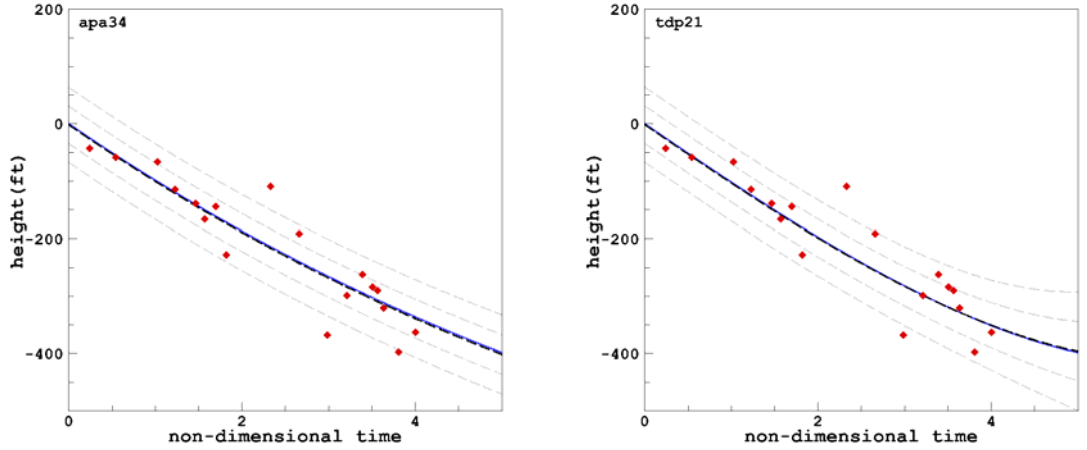

Figure 13. Run 37. Vortex descent predicted by APA34 and TDP21 models. Observations are given by the points, deterministic solution in blue, mean by the black dashed line and [σ:2σ] bounds by the dashed gray lines.

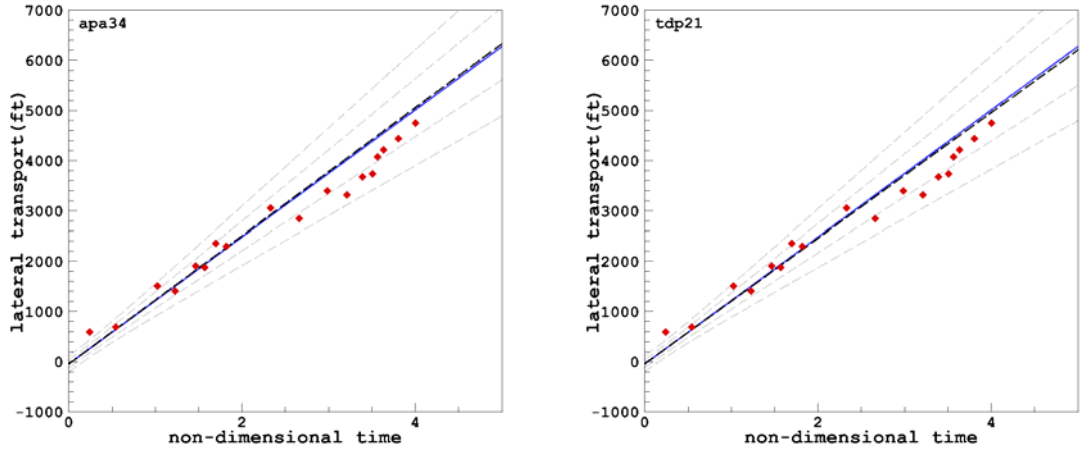

Figure 14. Run 37. Vortex transport predicted by APA34 and TDP21 models. Observations are given by the points, deterministic solution in blue, mean by black dashed line and [σ:2σ] bounds by the dashed gray lines.

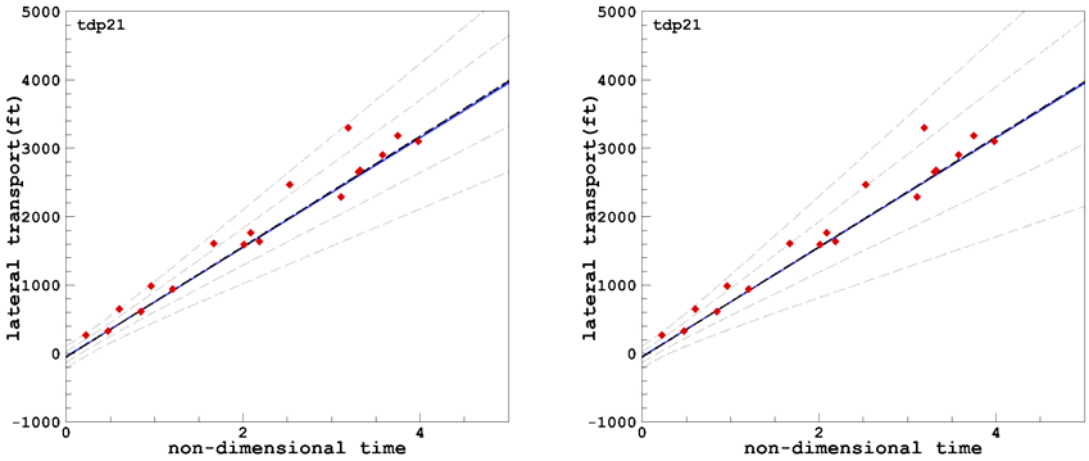

Figure 15. Run 28. Vortex transport predicted by TDP21 model. Observations are given by points, deterministic solution in blue, mean by black dashed line and [σ:2σ] bounds by the dashed gray lines. A 2σ value of 8.2ft/s was used for the figure shown in the left panel and a 2σ value of 12.5ft/s was used for the plot shown in the right panel.

C. Wake Encounters

The Bowles-Tatnall method (Appendix D) was used to estimate the vortex-induced rolling moment coefficient from the fast-time model prediction of circulation strength. The results for Run 28 are compared with C_{l_v} estimated from the observed decay curve in Figure 16 (left panel). Compared to APA3.4, the TDP2.1 predictions generally agreed well with observations with some discrepancies at later times due to prediction of faster decay compared to the decay rate estimated from observations.

A total of eighteen wake encounters were performed during Run 28, of which several were core encounters. The OV-10A response during encounter one (core encounter) of Run 28 is shown in Figure 16 (right panel). In this encounter, the OV-10A was moving right to left (0.3nmi in-trail of the generator). Flight test notes report that 'a lot of control was required to encounter'. The total encounter time was approximately 3s. As the aircraft penetrated the vortex from the side, the updraft induced a positive rolling moment on the left wing. The aircraft then moved into the vortex core region and the downdraft induced a negative rolling moment on the left wing. The pilot's reaction to the vortex-induced roll can be seen in the time history of the aileron deflection. The aircraft roll angle exceeded 40 degrees during the encounter.

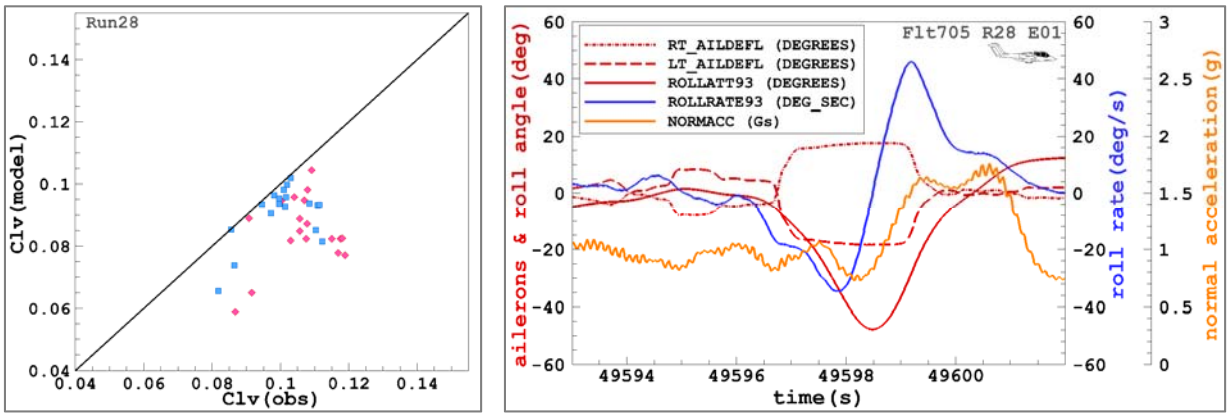

Figure 16. Comparison of vortex-induced rolling moment coefficient derived from circulation strength predicted by models (TDP21 in blue and APA34 in magenta) and calculated based on linear decay rate and methods defined in Appendix D is given in the right panel for all encounters of Run 28. $r_c = 0.05B_G$. The left panel shows the OV-10A response to one of the wake encounters during Run 28. Please note that 1*g* should be subtracted from the normal acceleration in the figure (accelerometers indicate 1*g* for level flight).

V. Summary

Integration of fast-time wake vortex models with flight data for ATM applications has been described in this paper. The newly developed system is capable of providing wake hazard bounds in terms of aircraft response to a wake upset. Previously, the wake models have been evaluated using lidar data. The methodology described in this study was used to evaluate the models using flight test data. The predictions of vortex location compared well with observations for both APA and the TDP models. The TDP prediction of circulation decay was more accurate than APA - which predicted faster decay than observations. Previous evaluations using lidar data have also shown more accurate predictions by TDP in stratified conditions. In addition, the National Center for Atmospheric Research's WRF model was used to evaluate mesoscale predictions of the potential temperature gradient with favorable results.

The data collected in Flight 705 were considered in this study. Future work will include evaluations using data from other flights as well. The vortex velocity field measured by the OV-10A during wake encounters was used to estimate the circulation decay of the wake. This methodology requires fitting the observed velocity field to a vortex model. Wake circulation can also be estimated using the response data of the encountering aircraft, which is a suitable topic for further model evaluation.

Appendix A: MacCready Turbulence Scale

The MacCready turbulence scale (MacCready 1964) is given in this appendix for reference. The scale was developed for aviation applications and is based on turbulence measurements taken from aircraft.

Table A1: MacCready Turbulence Scale

Category	ε (ft^2/s^3)	$\varepsilon^{1/3}$ ($ft^{2/3}/s$)
Negligible	<0.00024	<0.062
Light	0.00024-0.0032	0.062-0.147
Moderate	0.0032-0.045	0.147-0.356
Heavy	0.045-0.584	0.356-0.836
Extreme	>0.584	>0.836

Appendix B: Monte-Carlo Simulations

The general methodology used for performing Monte-Carlo simulations is described in this Appendix. The model initial conditions which can be perturbed include: ε, θ, u, b_0, V_0, z_0 and y_0. If the probability density functions are available, then they are utilized, otherwise uniform distributions are used within prescribed bounds. In case a varying vertical profile is used, then the profile is truncated at z_0 (height of vortex generation) and the mean is calculated from ground to z_0. Once the averages have been calculated, k perturbations are generated using the probability density functions. Uniform weather profiles are generated from these perturbations. Simulations are performed with all inputs, and the standard deviation and the mean are calculated for each time step. The standard deviation is then added and subtracted to the mean to create bounds for circulation strength and vortex location.

Two examples from the Memphis 1995 wake vortex field experiment (Campbell 1997) are given in this section. The weather probability density functions were obtained from the Memphis 1995 weather data. The initial conditions for Case 1995-08-10-233255 are given in Figure B1. The probability density functions are shown in Figure B2 (bottom row) and the perturbations introduced in the initial conditions are shown in Figure B2 (top row). Note that the generation of the theta profiles is done from the potential temperature gradient probability density function. Perturbations for y_0 are generated using a normal distribution with mean set to y_0 and σ=82ft (25m) (Holzäpfel 2013). Similarly for z_0, a normal distribution is used with mean set to z_0 and σ=23ft (7m). If the aircraft is in IGE, then σ is set to 13ft (4m). In these examples, the initial vortex spacing was assumed to be varying between $0.95b_0$ and b_0 (Holzäpfel 2013). Figure B3 shows the solution of 400 simulations (top row). The mean, bounds, deterministic APA34 solution and observations are shown in Figure B3 (bottom row). Figures B4-B6 show the results for Memphis case 1995-08-12-123930.

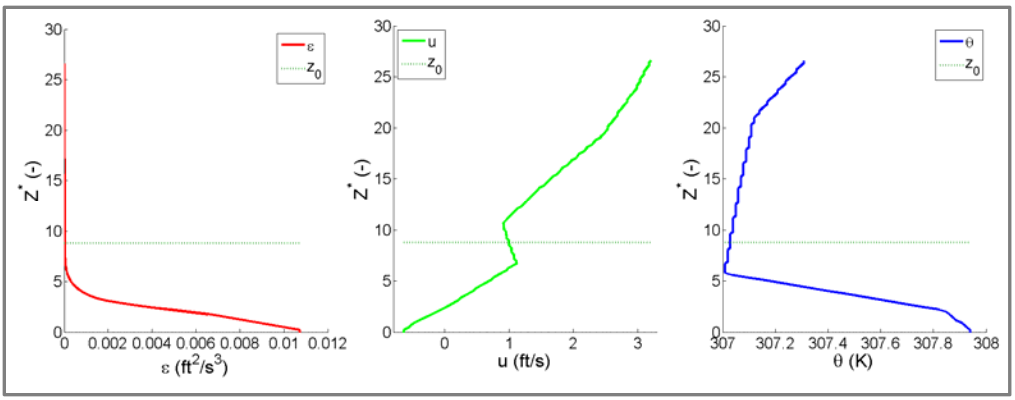

Figure B1. Case 1995-08-10-233255. EDR, crosswind and potential temperature initial conditions.

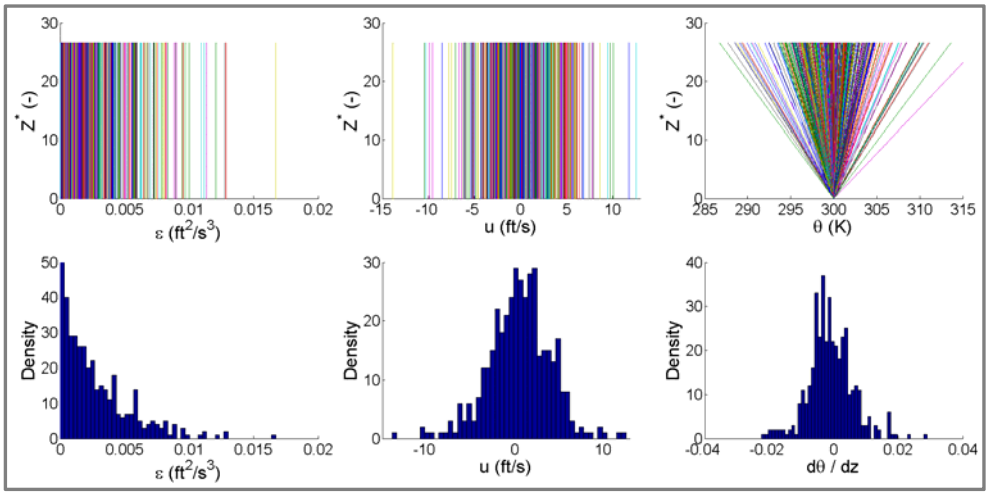

Figure B2. Case 1995-08-10-233255. Generated input profiles for EDR, crosswind and theta and the corresponding probability density functions.

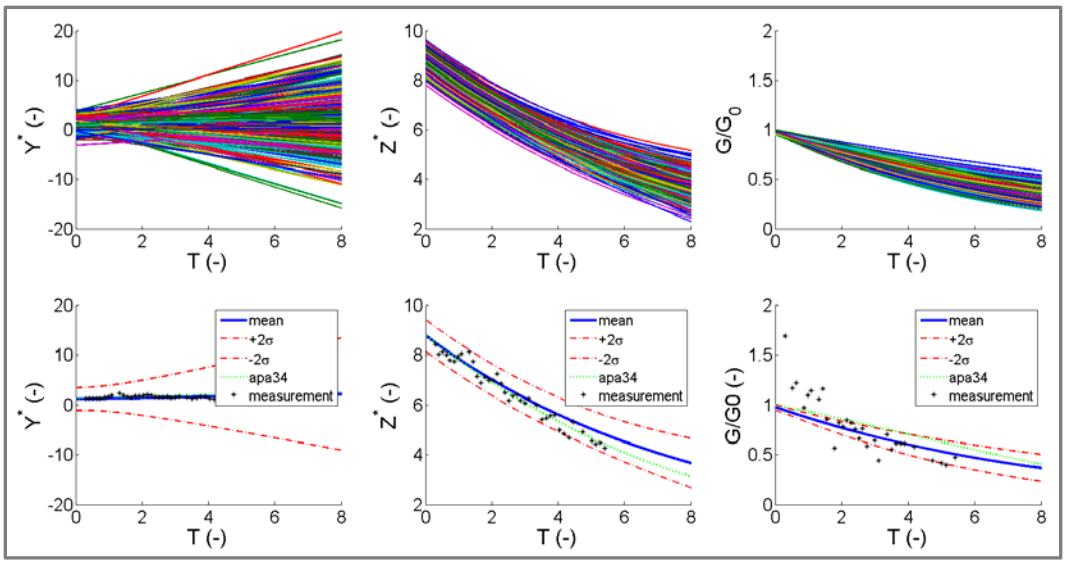

Figure B3. Case 1995-08-10-233255. The top row shows the results from all simulations. The bottom row shows the mean, and the bounds generated from the Monte-Carlo run.

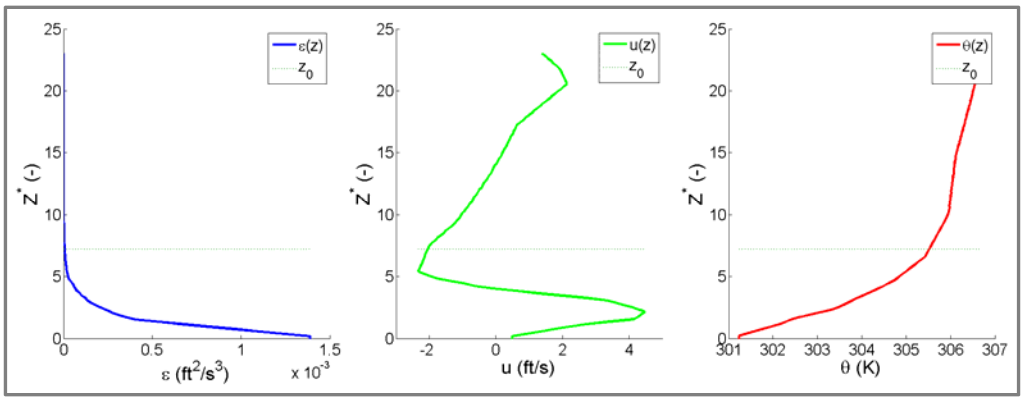

Figure B4. Case 1995-08-12-123930. EDR, crosswind and potential temperature initial conditions.

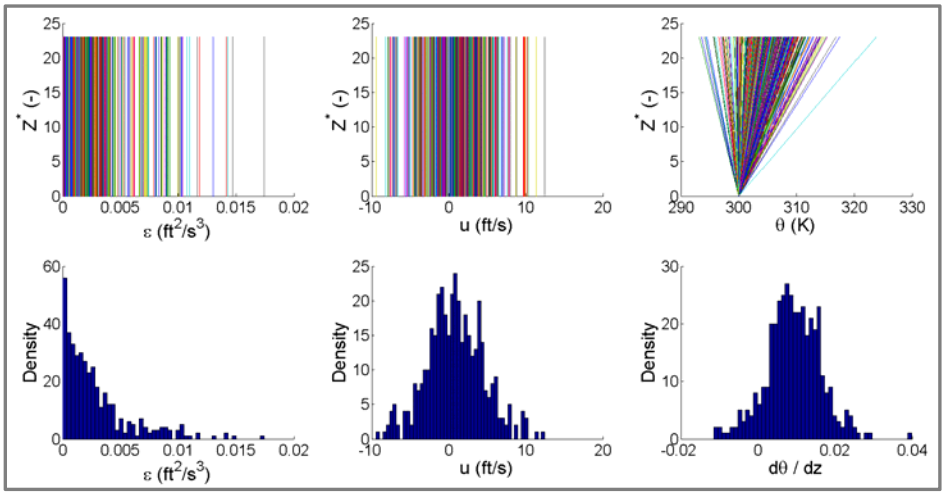

Figure B5. Case 1995-08-12-123930. Generated input profiles for EDR, crosswind and theta and the corresponding probability density functions.

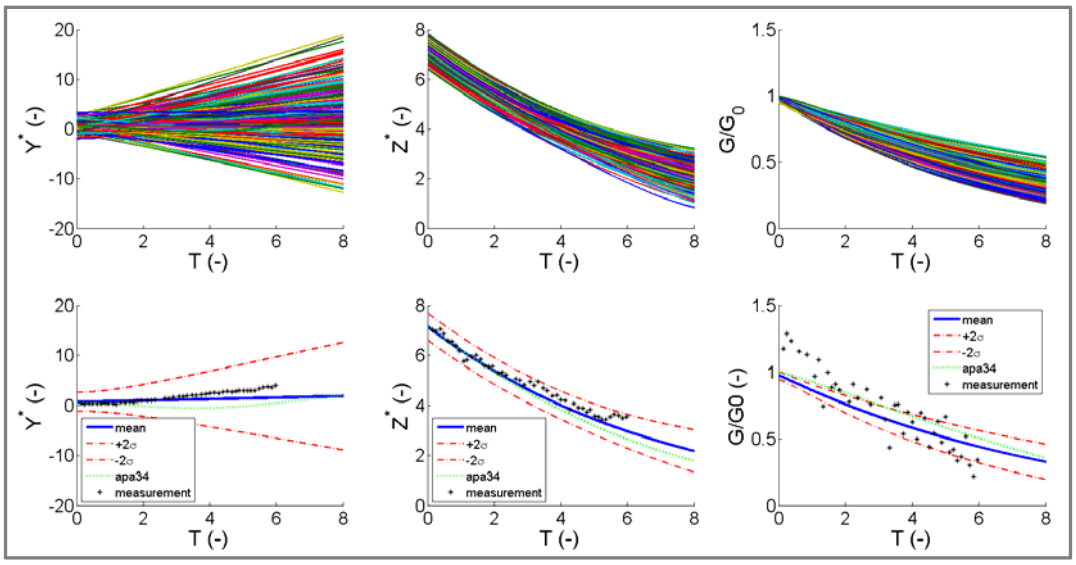

Figure B6. Case 1995-08-12-123930. The top row shows the results from all simulations. The bottom row shows the mean, and the bounds generated from the Monte-Carlo run.

Appendix C: Weather Research and Forecast (WRF) Model Simulations

The WRF model (Klemp et al. 2007) is a mesoscale numerical weather prediction model that has been developed by the National Center for Atmospheric Research in partnership with universities and federal agencies. It has governing equations for the time-dependent, three-dimensional, nonhydrostatic, fully compressible Navier-Stokes equations. The model uses higher-order schemes for spatial (second to sixth-order accuracy) and temporal discretizations. The time integration is done using an explicit third-order, Runge-Kutta time marching scheme, with time-splitting of acoustic and gravity wave modes to maintain numerical stability. The model grid structure is based on Arakawa C-grid staggering (Arakawa and Lamb 1977). In the vertical, WRF uses a terrain-following pressure formulation, where the top of the domain is a constant pressure surface. The grid can be stretched in the vertical to provide higher resolution in the boundary layer. In the horizontal direction, one-way and two-way nesting options are available to provide high grid resolution in regions of interest.

Monotonic as well as positive-definite schemes are available for the advection of scalars. The latest version of WRF (Version 3.4) includes the option for a fifth-order Weighted Essentially Non-Oscillatory (WENO) scheme (Liu et al. 1994) for the advection of microphysical scalars and turbulence kinetic energy (TKE). Extensive physics packages for modeling the surface layer interactions, boundary layer turbulence and microphysical processes have been implemented in the model.

Several simulations were conducted to evaluate the prediction of potential temperature gradient. The WRF simulation domain consisted of an outermost domain bounded between 91.63°W and 59.56°W in longitude and 26.41°N and 47.88°N in latitude with a mesh resolution of 9km. Two higher resolution nests (3km and 1km) were defined within the outermost domain. The WRF computational domain and the terrain for the innermost nest are shown in Figure C1. The fifth-order upwind-biased scheme was used in the horizontal and the third-order upwind-biased scheme was used in the vertical within a three-stage Runge-Kutta explicit time-marching scheme. The Rapid Radiative Transfer Model (RRTM) longwave radiation scheme (Mlawer et al. 1997) and the Goddard shortwave scheme (Chou and Suarez 1999) were used to parameterize the effects of both the longwave and the shortwave radiative transfer in the atmosphere. The Thompson scheme (Thompson et al. 2004) was used for the microphysics, and the cumulus parameterization schemes were switched off for the simulations. The Mellor-Yamada-Janjić turbulence scheme (Janjić 1994) was used to parameterize subgrid scale turbulent processes. A fifth-order WENO scheme with positive definite limiter was used to transport microphysical scalars as well as turbulence kinetic energy.

The simulations were initialized for August 13, 1997 at 0000UTC using the North American Regional Reanalysis (Mesinger et al. 2006) data and run for a 24hr forecast. Data from the high-resolution 1km nest were output every 15min.

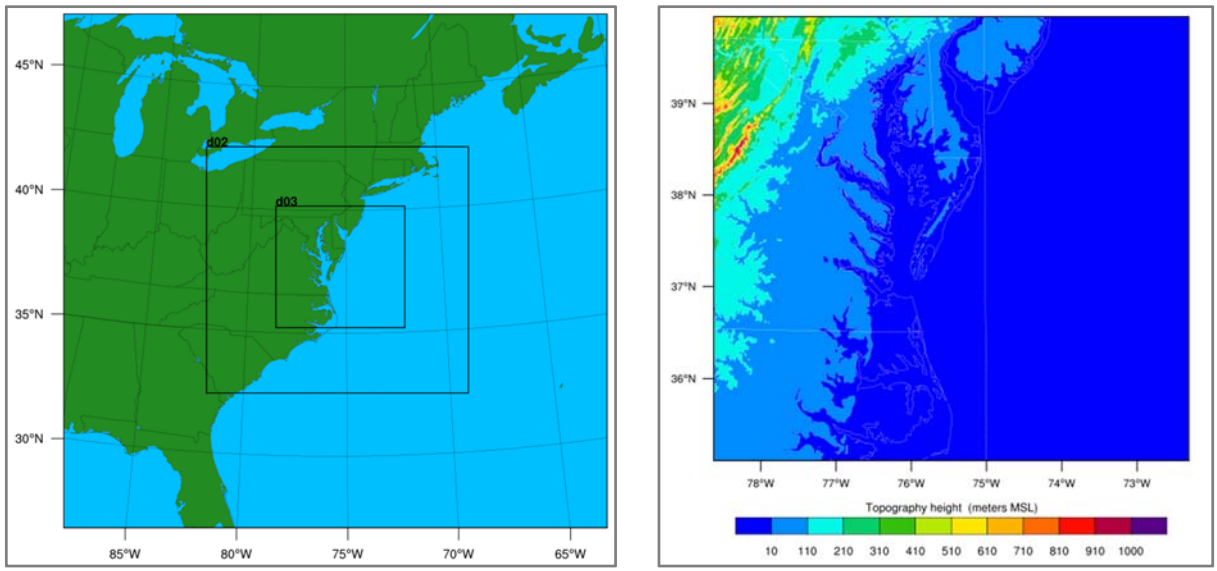

Figure C1. The WRF computational domain with higher resolution nests (left panel). The innermost nest had a resolution of 1*km*. The terrain heights for the innermost nest are shown in the right panel.

Figure C2 shows the comparison of simulated temperature profile with the special soundings launched from the Wallops Flight Facility at three different times to support Flight Test 705. There are small discrepancies between forecasted and measured temperature near the surface but the WRF simulation is in excellent agreement with soundings at higher altitudes where the flight tests were conducted. Figure C3 shows the comparison of WRF predicted potential temperature with measurements taken by OV-10A during the four weather runs. Although there are differences in the magnitude of the WRF predicted potential temperature and the OV-10A measured potential temperature, the gradients agree well. The fast-time wake models use the potential temperature gradient in wake decay calculations.

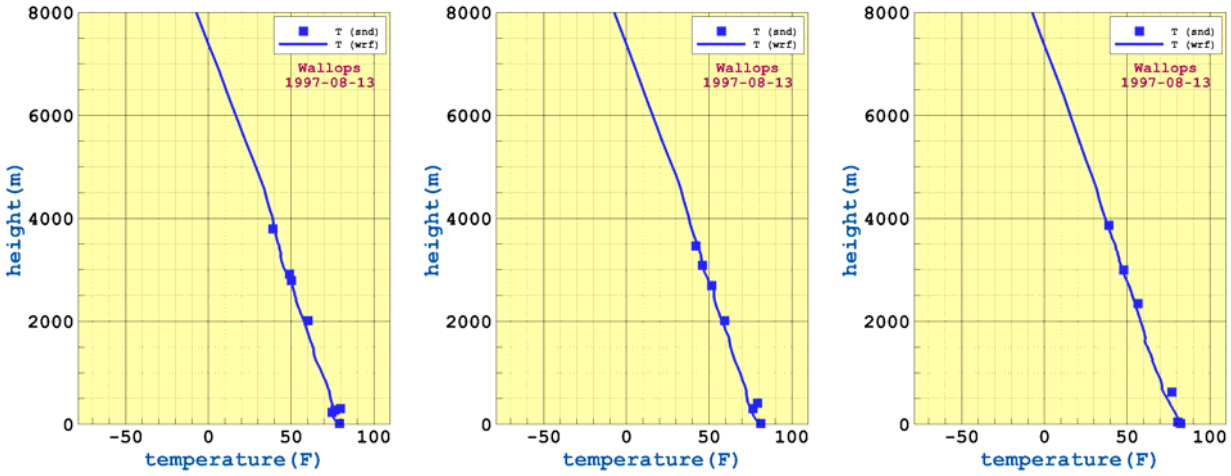

Figure C2. Comparison of WRF simulation with observations. 1300UTC (left), 1400UTC (middle) and 1500UTC (right). WRF simulation results are denoted by solid lines. The soundings were launched from the Wallops Flight Facility to support the flight test.

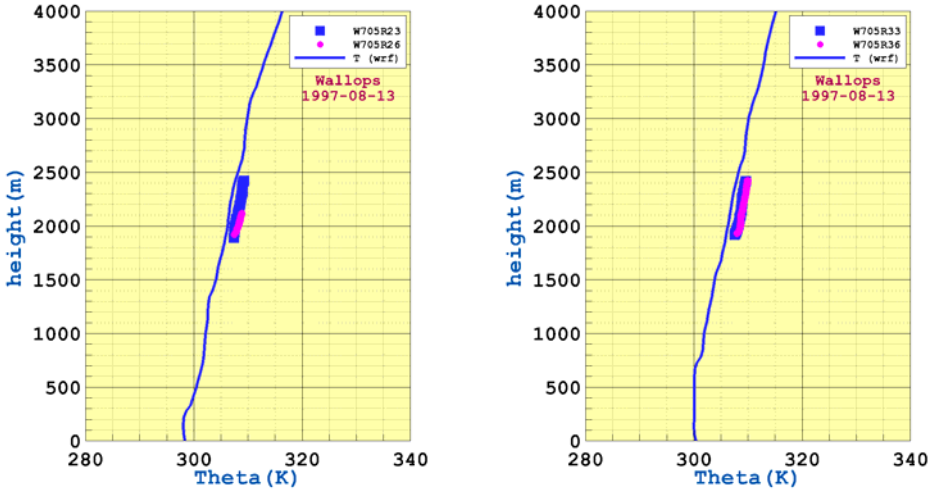

Figure C3. Comparison of WRF simulation with the OV-10A weather runs. 1325UTC (left) and 1445UTC (right). WRF simulation results are denoted by solid lines.

Appendix D: Bowles-Tatnall Method

Several wake encounter metrics have been proposed in the past (Van der Geest 2012) but no standard has been defined to date. These metrics include the rolling moment coefficient, bank angle, and roll control ratio. The vortex-induced rolling moment coefficient was recently used by Lang et al (2010) in their analysis of re-categorization of wake categories. Lang et al. (2010) noted that, "rolling moment coefficients of 0.05 to 0.07 are the maximum that can be controlled by the roll control authority of an aircraft using ailerons only, and that larger rolling moments might exceed an aircraft's roll control authority." The Bowles-Tatnall method (Tatnall 1995) was used in this study to determine vortex-induced rolling moment coefficient. The method was chosen because it is available in open literature, has gone through validation and is easy to interface with fast-time model prediction of circulation strength. The method is described in detail in Tatnall (1995) along with a validation study using data from wind tunnel experiments and flight tests.

A. Vortex-Induced Rolling Moment Coefficient, C_{l_v}

The vortex-induced rolling moment coefficient, C_{l_v} can be written as:

$$C_{l_v} = K_{l_v}\left(I_1 - I_2\right), \tag{D.1}$$

where,

$$K_{l_v} = \left(\frac{\Gamma_0}{\pi}\right)\left(\frac{C_{L_\alpha F} b_G}{b_F^2 V_F}\right)\left(\frac{1}{1+\lambda_F}\right). \tag{D.2}$$

In Eq. (D.2), Γ_0 is the initial circulation strength of the generator, b_G is the wingspan of the generator, $C_{L_\alpha F}$ is the three-dimensional lift curve slope of the follower, b_F is the wingspan of the follower, V_F is the follower airspeed, and λ_F is the follower wing taper ratio. I_1 and I_2 are defined as follows:

$$\begin{aligned} I_i = {} & \frac{1}{2}\left[\left(C_i^2 - A_i^2\right)\Omega - C_i\right]\ln\left[\frac{C_i^2 + A_i^2}{(C_i - B)^2 + A_i^2}\right] + \frac{1}{2}\left[\left(C_i^2 - A_i^2\right)\Omega - C_i\right]\ln\left[\frac{C_i^2 + A_i^2}{(C_i + B)^2 + A_i^2}\right] + \\ & A_i\left[4C_i\Omega\tan^{-1}\left(\frac{C_i}{A_i}\right) + \left(1 - 2C_i\Omega\right)\tan^{-1}\left(\frac{C_i - B}{A_i}\right) - \left(1 + 2C_i\Omega\right)\tan^{-1}\left(\frac{C_i + B}{A_i}\right)\right] \quad i = 1,2 \end{aligned} \tag{D.3}$$

The parameters, C_1, C_2, A_1, A_2, B, and Ω in the above equations are defined as follows:

$$C_1 = \left(\bar{Y}_F + \bar{s}\right)\cos(\phi) + \bar{Z}_F \sin(\phi), \tag{D.4}$$

$$C_2 = \left(\bar{Y}_F - \bar{s}\right)\cos(\phi) + \bar{Z}_F \sin(\phi), \tag{D.5}$$

$$A_1^2 = \left[\left(\bar{Y}_F + \bar{s}\right)\sin(\phi) - \bar{Z}_F \cos(\phi)\right]^2 + \bar{r}_c^2, \tag{D.6}$$

$$A_2^2 = \left[\left(\bar{Y}_F - \bar{s}\right)\sin(\phi) - \bar{Z}_F \cos(\phi)\right]^2 + \bar{r}_c^2, \tag{D.7}$$

$$B = \frac{b_F}{2b_G}, \tag{D.8}$$

$$\Omega = \frac{1 - \lambda_F}{B}. \tag{D.9}$$

In Eq. (D.4)-(D.7), ϕ is the bank angle of the follower, $\overline{Y}_F$ is the *y*-coordinate of follower's center of gravity normalized by b_G, $\overline{Z}_F$ is the *z*-coordinate of follower's center of gravity normalized by b_G, $\bar{s}$ is the half of vortex pair separation (b_0) normalized by b_G, and $\bar{r}_c$ is the vortex core radius size normalized by b_G.

B. Calculation of C_{l_v} at Time *t*

The vortex-induced rolling moment coefficient as a function of time is related to the circulation strength decay by the following relation (Tatnall 1995):

$$C_{l_v}(t) = \frac{\Gamma(t)}{\Gamma(0)} C_{l_v}(0), \tag{D.10}$$

where, $C_{l_v}(0)$ is the vortex-induced rolling moment coefficient due to initial vortex circulation strength $\Gamma(0) = \Gamma_0$.

C. Maximum Vortex-Induced Roll Angle, ϕ_{max}

The vortex-induced maximum roll angle can be approximated using a one degree-of-freedom (1DoF) model (Tatnall 1995):

$$\phi_{\max} = \phi_\infty \left[1 + \frac{R(T_c - T_m)}{T_v} \right], \tag{D.11}$$

where, $\phi_\infty = -\dfrac{K_1 C_{l_v} T_v}{K_2}$, is the maximum bank angle of the aircraft without control input. The dynamic pressure *q*, and, the parameters, K_1, K_2 and, R are given by:

$$K_1 = \frac{qS_F b_F}{I_{xx}}; \qquad K_2 = \frac{K_1 C_{l_{\bar{p}}} b_F}{2V_F}; \qquad R = \frac{C_{l_c}}{C_{l_v}}; \qquad q = \frac{\rho V_F^2}{2}. \tag{D.12}$$

The time at which the bank angle reaches a maximum is given by:

$$T_m = -\frac{1}{K_2} \ln\left(\frac{R e^{-K_2 T_c} + e^{-K_2 T_v} - 1}{R} \right). \tag{D.13}$$

In Eq. (C.12), $C_{l_c} = 0.07 \left| C_{l_{\bar{p}}} \right|$ is the pilot input roll control corresponding to maximum aileron deflection, and $C_{l_{\bar{p}}}$ is the roll damping coefficient of the follower. T_c is the time of control input activation and, T_v is the time of vortex impulse deactivation, and I_{xx} is the roll moment of inertia.

The Bowles-Tatnall method requires several aircraft parameters which may not be readily available. These parameters include the three-dimensional lift curve slope of the follower, the pilot input roll control corresponding to maximum aileron deflection, the roll damping coefficient of the follower, and the roll moment of inertia of the follower, etc. A database of these parameters for a small set of different aircraft is given in Tatnall (1995).

Acknowledgments

Many thanks to Dan Vicroy for providing the flight test data and for helpful discussions on the flight tests. This work is sponsored under NASA's Concepts and Technology Development Project of the Airspace Systems Program. The WRF model simulations were conducted on NASA Langley's K-cluster.

References

Ahmad, N.N., R.L. VanValkenburg, M.J. Pruis, "NASA AVOSS Fast-Time Wake Prediction Models: User's Guide", National Aeronautics and Space Administration, 2014, NASA/TM-2014-218152.

Ahmad, N.N., F.H. Proctor, R.L. VanValkenburg, M.J. Pruis, F. Duparcmeur, "Mesoscale Simulation Data for Initializing Fast-Time Wake Transport and Decay Models," AIAA Paper 2013-0429.

Arakawa, A., V. R. Lamb, "Computational design of the basic dynamical process of the UCLA general circulation model", *Methods in Computational Physics*, Vol. 17, 1977, pp. 173-265.

Campbell, S.D., et al., "Wake Vortex Field Measurement Program at Memphis, TN Data Guide", Lincoln Laboratory, Massachusetts Institute of Technology. Project Report NASA/L-2. 1997.

Chou, M. D., and M. J. Suarez, "A solar radiation parameterization for atmospheric studies", NASA Technical Report NASA/TM-1999-10460. 1999.

Delisi, D.P., M.J. Pruis, F.Y. Wang, D.Y. Lai, "Estimates of the Initial Vortex Separation Distance, b_0, of Commercial Aircraft from Pulsed Lidar Data," AIAA Paper 2013-0365.

Feigh, K.M., L. Sankar, V. Manivannan, "Statistical Determination of Vertical Resolution Requirements for Real-Time Wake-Vortex Prediction", *Journal of Aircraft*, Vol. 49, 2012, pp. 822-835.

Gerz, T., F. Holzäpfel, W. Bryant, F. Köpp, M. Frech, A. Tafferner, G. Winckelmans, "Research towards a wake vortex advisory for optimal aircraft spacing", *Journal of Applied Meteorology and Climatology*, Vol. 46, 2007, pp. 1913-1932.

Greene, G.C., "An Approximate Model of Vortex Decay in the Atmosphere", *Journal of Aircraft*, Vol. 23, 1986, pp. 566-573.

Han, J. Y.L. Lin, S.P. Arya, F.H. Proctor, "Numerical study of wake vortex decay and descent within homogeneous turbulence," *AIAA Journal*, Vol. 38, 2000, pp. 643- 656.

Holzäpfel, F., "Sensitivity Analysis of the Effects of Aircraft and Environmental Parameters on Aircraft Wake Vortex Trajectories and Lifetimes", AIAA Paper 2013-0363.

Holzäpfel, F., "Probabilistic Two-Phase Wake-Vortex Decay and Transport Model," *Journal of Aircraft*, Vol. 40, 2003, pp. 323-331.

Hinton, D.A., "Description of Selected Algorithms and Implementation Details of a Concept-Demonstration Aircraft Vortex Spacing System (AVOSS)," NASA TM-2001-211027.

Janjić, Z., "The Step-Mountain Eta Coordinate Model: Further Developments of the Convection, Viscous Sublayer, and Turbulence Closure Schemes", *Monthly Weather Review*, Vol. 122, 1994, pp. 927-945.

Johnson, S. et al., "Simplified Aircraft-Based Paired Approach: Concept Definition and Initial Analysis", NASA/TP-2013-217994.

Klemp, J.B., W.C. Skamarock, and J. Dudhia, "Conservative Split-Explicit Time Integration Methods for the Compressible Nonhydrostatic Equations," *Monthly Weather Review*, Vol. 135, 2007, pp. 2897-2913.

Lang, S., J. Tittsworth, W.H. Bryant, P. Wilson, C. Lepadatu, D.P. Delisi, D.Y. Lai, G.C. Greene, "Progress on an ICAO Wake Turbulence Re-Categorization Effort", AIAA Paper 2010-7682.

Liu, X., S. Osher, and T. Chen, "Weighted Essentially Non-Oscillatory Schemes," *Journal of Computational Physics*, Vol. 115, 1994, pp. 200-212.

MacCready, P.B., "Standardization of Gustiness Values from Aircraft," *Journal of Applied Meteorology*, Vol. 3, 1964, pp. 439-449.

Mesinger, F., G. DiMego, E. Kalnay, K. Mitchell, P. C. Shafran, W. Ebisuzaki, D. Jović, J. Woollen, E. Rogers, E. H. Berbery, M. B. Ek, Y. Fan, R. Grumbine, W. Higgins, H. Li, Y. Lin, G. Manikin, D. Parrish, W. Shi, "North American Regional Reanalysis," *Bulletin of the American Meteorological Society*, Vol. 87, 2006, pp. 343-360.

Mlawer, E. J., S. J. Taubman, P. D. Brown, M. J. Iacono, and S. A. Clough, "Radiative transfer for inhomogeneous atmosphere: RRTM, a validated correlated-k model for the longwave", *Journal of Geophysical Research*, Vol. 102, 1997, pp. 663-682.

Perry, R.B., D.A. Hinton, R.A. Stuever, “NASA Wake Vortex Research for Aircraft Spacing,” AIAA Paper 1997-0057.

Proctor, F.H., Hamilton, D.W. and Han, J., “Wake Vortex Transport and Decay in Ground Effect: Vortex Linking with the Ground,” AIAA-2000-0757.

Proctor, F. H., "The Terminal Area Simulation System / Volume 1: Theoretical Formulation," NASA/CR 1987-4046.

Proctor, F. H., "The Terminal Area Simulation System / Volume 2: Verification Cases," NASA/CR 1987-4047.

Proctor, F.H., D.W. Hamilton, G.F. Switzer, “TASS Driven Algorithms for Wake Prediction”, AIAA Paper 2006-1073.

Proctor, F.H., “Evaluation of Fast-Time Wake Vortex Prediction Models”, AIAA Paper 2009-0344.

Pruis, M.J., D.P. Delisi, N.N. Ahmad, “Comparisons of Crosswind Velocity Profile Estimates Used in Fast-Time Wake Vortex Prediction Models,” AIAA Paper 2011-1002.

Pruis, M.J., D.P. Delisi, “Comparison of Ensemble Predictions of a New Probabilistic Fast-Time Wake Vortex Model and Lidar Observed Vortex Circulation Intensities and Trajectories,” AIAA Paper 2011-3036.

Pruis, M.J., D.P. Delisi, “Assessment of Fast-Time Wake Vortex Prediction Models using Pulsed and Continuous Wave Lidar Observations at Several Different Airports,” AIAA Paper 2011-3035.

Reimer, H.M., D.D. Vicroy, “A Preliminary Study of a Wake Vortex Encounter Hazard Boundary for a B737-100 Airplane,” NASA/TM-1996-110223.

Robins, R.E., Delisi, D.P., and Greene, G.C., “Algorithm for Prediction of Trailing Vortex Evolution,” *Journal of Aircraft*, Vol. 38, 2001, pp. 911-917.

Robins, R.E., and D.P. Delisi, “NWRA AVOSS Wake Vortex Prediction Algorithm Version 3.1.1,” NASA CR 2002-211746.

Sarpkaya, T., “New Model for Vortex Decay in the Atmosphere,” *Journal of Aircraft*, Vol. 37, 2000, pp. 53-61.

Sarpkaya, T., R.E. Robins, and D.P. Delisi, “Wake-Vortex Eddy-Dissipation Model Predictions Compared with Observations,” *Journal of Aircraft*, Vol. 38, 2001, pp. 687- 692.

Stuever, R.A., E.C. Stewart, R.A. Rivers, “Overview of the Preparation and Use of an OV-10 Aircraft for Wake Vortex Hazards Flight Experiments”, AIAA Paper 1995-3935.

Tatnall, C.R.,”A Proposed Methodology for Determining Wake-Vortex Imposed Aircraft Separation Constraints”, M.S. Thesis, George Washington University, 1995.

Thompson, G., R. M. Rasmussen, K. Manning, “Explicit Forecasts of Winter Precipitation using an Improved Bulk Microphysics Scheme. Part1: Description and Sensitivity Analysis”, *Monthly Weather Review*, Vol. 132, 2004, pp. 519-542.

van der Geest, P., “Wake vortex severity criteria: The search for a single metric”, NLR Air Transport Safety Institute, February 2012.

Vicroy, D.D., and R.A. Stuever, E.C. Stewart, R.A. Rivers, “Flight Data Reduction of Wake Velocity Measurements Using an Instrumented OV-10 Airplane,” NASA/TM-1999-209552.

Vicroy, D.D., P.M. Vijgen, H.M. Reimer, J.L. Gallegos, P.R. Spalart, “Recent NASA Wake-Vortex Flight Tests, Flow Physics Database and Wake-Development Analysis,” AIAA Paper 1998-5592.

de Visscher, I., G. Winckelmans, T. Lonfils, L. Bricteux, M. Duponcheel, N. Bourgeois, “The WAKE4D simulation platform for predicting aircraft wake vortex transport and decay: Description and examples of application,” AIAA Paper 2010-7994.

Zak, J.A., and W.G. Rodgers, “Documentation of Atmospheric Conditions During Observed Rising Aircraft Wakes,” NASA/CR-1997-4767.